Proceedings of International Conference on Heat Exchanger Fouling and Cleaning - 2011 (Peer-reviewed)
June 05 - 10, 2011, Crete Island, Greece
Editors: M.R. Malayeri, H. Müller-Steinhagen and A.P. Watkinson

Published online
www.heatexchanger-fouling.com

DEVELOPMENT OF A PREDICTIVE CFD FOULING MODEL FOR DIESEL ENGINE EXHAUST GAS SYSTEMS

M. C. Paz, E. Suárez, A. Eirís and J. Porteiro

CFD Simulation Group, University of Vigo, Lagoas Marcosende 9, CP-36310 Vigo (Spain) cpaz@uvigo.es

ABSTRACT

This paper presents a numerical simulation procedure for studying soot particle deposition in diesel exhaust systems, with a particular focus on fouling layer thickness evolution.

In the proposed algorithm, particle transport towards the wall, adhesion and re-entrainment of particles from the surface have been modelled, including Brownian motion and turbulent diffusion, thermophoresis, adhesion and removal. This model has been implemented in ANSYS Fluent, which makes the inclusion of local effects possible.

A cross-flow device, with a tube positioned transverse to the flow, has been simulated and tested. A comparison of the predicted fouling layer at several angular positions with the experimental observation shows acceptable agreement.

This model makes it possible to predict the real depth of the fouling layer and its effects on the hydrodynamics of the flow. This model represents a valuable tool for the prediction of the main aspects of the performance of heat exchangers exposed to fouling.

INTRODUCTION

In recent years, the requirements imposed on exhaust systems have become increasingly severe. These requirements apply to turbochargers, intercoolers, catalysts, regenerators, filters, heat exchangers, and a growing number of antipollution devices. All these systems have a common problem: they are damaged by fouling effects, and fouling is one of the most important design considerations in exhaust gas systems.

The deposition of fouling material on a heat transfer surface decreases thermal efficiency (Marner, 1990) because of the additional resistance to heat transfer from the hot to the cool side. In most cases, this additional layer means a significant reduction in the transverse flow cross-section, which causes an increase in the gas pressure drop.

The examination of wall deposits has shown that particulate matter and hydrocarbons are the main constituents of the fouling layer (Hoard et al., 2008), and soot particle deposition is the most important mechanism of fouling (Grillot and Icart, 1997). The growth of the soot layer is driven by different physical mechanisms: thermophoresis, Brownian motion, gravitational settling or electrostatic forces, which depend on the nature and size of the particles and on the operating conditions. The typical soot particle size in diesel exhaust gases is on the order of 10^1~10^2 nm (Chandler et al., 2007), for which thermophoretic force is the most important deposition force when thermal gradients are present.

Information about fouling effects in diesel exhaust gas systems is normally obtained from experimental data, so any predictive tool will provide a significant advance in exhaust system design. The aim of the current study was to develop a semi-empirical fouling model that takes into account local effects. The model has been implemented by coupling an external algorithm programmed in C++ to the commercial CFD software package ANSYS-FLUENT 6.3.26 via the user-defined function (UDF) feature.

The starting point of fouling dynamics modelling was the well-known Kern and Seaton approach (1959), which postulates that the net growth of the soot layer depends on the relative contribution of two opposing simultaneous processes: deposition and removal. This approach has been accepted by most of the research community and was enhanced later by Kim and Webb (1991). The use of this type of model represents an advance in design that focuses on functionality and ease of application for practical problems.

The local scale effects involved into fouling process are accounted thanks to the formulation proposed. Regarding the development of numerical models, there are different ways to approach the problem. Most of the published works employ a virtual deposited mass that changes the conductivity of a constant-thickness wall to incorporate the fouling effect. With this approach, the reduction of the flow area and the modification of the flow pattern cannot be taken into account.

In deposition studies, the Euler-Euler models have been extended from the first simple free-flight model of Friedlander and Johnstone (1957) to more recent works, including the Eulerian turbophoretic models of Guha (1997) and Young and Leeming (1997). The Euler-Lagrange models are categorised by the turbulent treatment used in the RANS-, LES- and DNS-Lagrange models. The Euler-0D model offers a reduced computational effort but requires experimental correlations to be as similar as possible to the situation being simulated.

No definitive theory currently exists for the removal of fouling material. Many researchers have tried to formulate the re-entrainment mechanism (Adhiwidjaja et al., 2000; Matsusaka et al., 1997) by analysing the torque and forces exerted on the deposited particles, measuring the removal efficiency of re-entrainment of particles, (Theerachaisupakij et al., 2003), or evaluating the influence of the velocity magnitude or the flow direction in the removal process (Abd-Elhady et al., 2009).

FOULING EVOLUTION

The mean soot layer thickness and resistance for the heat transfer surface are normally included in the calculation of the thermal performance of the heat exchangers using the fouling factor, which is shown in Eq. (1).

$$FF = \frac{1}{U_f} - \frac{1}{U_c} \tag{1}$$

The typical temporal fouling evolution on the exhaust gas side follows the asymptotic profile shown in Fig. 1. Several researchers, such as Bott (1995), Grillot and Icart (1997) and others (Müller-Steinhagen and Middis, 1989; Paz et al., 2009; Thonon et al., 1999), support this hypothesis.

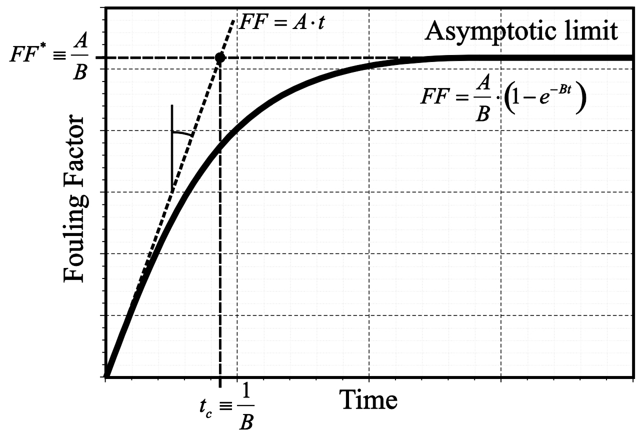

Fig. 1 Temporal evolution of the fouling factor.

Numerically, this type of evolution can be expressed by a differential equation, which is shown in Eq. (2):

$$\frac{d(FF)}{dt} = A - B \cdot FF \tag{2}$$

where A>0 and B>0. Separating the variables and integrating, a general solution is obtained, which is shown in Eq. (3):

$$FF = \frac{A}{B} \pm \frac{K}{B} \cdot e^{-Bt} \tag{3}$$

where K is the integration constant.

This solution represents a family of asymptotic curves, where FF approaches the asymptote $FF=A/B$ when $t \rightarrow \infty$.

Using the initial condition $FF_{(t=0)} = \frac{A}{B} \pm \frac{K}{B}$ and the specific case of $FF_{(t=0)}=0$, we find that $K=-A$. Therefore, the particular solution is shown in Eq. (4).

$$FF = \frac{A}{B} \cdot \left(1 - e^{-Bt}\right) \tag{4}$$

The fouling temporal evolution is defined by Eq. (4). An analysis of this equation is shown in Fig. 1. The asymptotic value, when $t \rightarrow \infty$, is A/B. The initial slope of the fouling curve is A (found by setting $t=0$ in Eq. (2)), so the origin tangent line is $FF=A\cdot t$.

Another important value is the intersection of the asymptotic line ($FF=A/B$) with the origin tangent line ($FF=A\cdot t$). This intersection occurs at $t=1/B$ and is defined as the characteristic time. Defining A/B as the asymptotic fouling factor FF^* and $1/B$ as the characteristic time t_c, Eq. (4) can be rewritten as Eq. (5):

$$FF = FF^* \cdot \left(1 - e^{-\frac{t}{t_c}}\right) \tag{5}$$

FOULING MODEL

A specific fouling model has been developed and experimental validation has been performed for a diesel exhaust gas system.

Most of the fouling studies in the literature assume that deposit accumulation is the result of two simultaneous, opposing events, deposition and removal, and that the net fouling rate is the difference between them. Kern and Seaton (1959) proposed a fouling model applicable to asymptotic fouling, with a constant deposition rate, m_d, and an increasing removal rate, $\dot{m}_r$. The $\dot{m}_r$ was assumed to be directly proportional to the mass of the fouling deposit per unit area and wall shear stress.

The presented model is a semi-empirical and phenomenological model that is in accordance with deposition-removal–type models (Epstein, 1997; Kern and Seaton, 1959; Kim and Webb, 1991). This model makes it possible to predict fouling layer evolution on a local scale with two adjusted parameters: the sticking probability S_d introduced by Epstein (1997) and the strength bond factor ξ. The effective fouling layer growth velocity, v^+_{eff}, is defined as the difference between the dimensionless deposition and removal velocities, as shown in Eq. (6).

$$v^+_{eff} = u^+_d - u^+_r = u^+_{d\,i} + u^+_{th} - u^+_r \tag{6}$$

The expressions for the deposition and removal velocities in the proposed model needed to be formulated to account for the specific mechanisms of deposition and erosion that govern fouling in the studied systems. Deliberately, the model can accommodate different fouling mechanisms, provided the fouling is asymptotic. Thus, the model can be used to analyse real fouling conditions, including the complex deposition and removal mechanisms associated with u^+_d and u^+_r. The deposition velocity has been considered to be the result of two contributions: the dimensionless deposition velocity under isothermal conditions, u^+_{di}, and the thermophoretic dimensionless deposition velocity, u^+_{th}.

The dimensionless deposition velocities were obtained with the friction velocity u_τ, calculated locally by the CFD program. The dimensionless expressions are defined as follows:

• u^+_{di} is the dimensionless deposition velocity using the Wood correlation (Wood, 1981) (Eq. (7))

$$u^+_{di} = 0.057 \cdot Sc^{-2/3} + 4.5 \cdot 10^{-4} \tau^{+2} \tag{7}$$

• u^+_{th} is the thermophoretic velocity taken from Talbot et al., (1980) (Eq. (8)). Several experimental studies suggested that the thermophoretic coefficient proposed by Talbot is sufficiently accurate (Tsai and Lu, 1995).

$$u^+_{th} = -\frac{2C_S}{1+3C_m \cdot Kn} \cdot \frac{\frac{\lambda_g}{\lambda_p} + C_t \cdot Kn}{1 + 2 \cdot \frac{\lambda_g}{\lambda_p} + 2C_t \cdot Kn} \cdot \frac{\upsilon \cdot C_C \cdot \nabla T}{u_\tau \cdot T} \tag{8}$$

$$C_C = 1 + \frac{2l}{d_p}\left(1.257 + 0.4 \cdot e^{1.1 d_p / 2l}\right) \tag{9}$$

where $Sc=\upsilon/D$ is the Schmidt number and $D = \frac{K_B T}{3\pi\mu d_p}$ is the mass diffusion coefficient; the constants are $C_S=1.17$, $C_t=2.18$ and $C_m=1.14$, and C_C (Eq. (9)) is the Stokes-Cunningham slip correction factor (Friedlander, 1977).

Regarding the removal term, Eq. (10), there is experimental evidence that the major part of the deposit was formed in areas where shear forces were low (Bouris et al., 2005; Bott, 1995; Kim and Webb, 1991). Additionally, the assumption that the shear action is the most important effect influencing the fouling removal has been made by several researchers for diesel exhaust systems (Abarham et al., 2010). In this work, the removal rate is assumed to be directly proportional to the fouling thickness, x_f, and local wall shear stress, τ_w, and inversely proportional to the strength bond factor, ξ. The local wall shear stress, τ_w, was calculated by the CFD program, and the fouling thickness, x_f, was iteratively calculated externally using the fouling model.

$$u^+_r = \frac{\tau_w \cdot x_f}{\xi \cdot u_\tau} = \frac{\rho \cdot u_\tau \cdot x_f}{\xi} \tag{10}$$

The temporal fouling thickness evolution could be easily obtained from the effective growth velocity, rearranged in Eq. (11), for which all of the variables should be known. The complete scheme of the equations used is shown in Fig. 2.

$$\Delta x_f = \left(\frac{S_d \cdot \left(u_{d\,i} + u_{th}\right) \cdot C_b}{\rho_f} - \frac{\tau_w \cdot x_f}{\xi} \right) \cdot \Delta t \tag{11}$$

where the strength bond factor ξ is given by:

$$\xi = a_1 - \left(\frac{a_1 - a_2}{1 + e^{a_3(\tau_w - a_4)}} \right) \tag{12}$$

In the above expression, a_i values are experimentally fitted constants (Suárez et al., 2010).

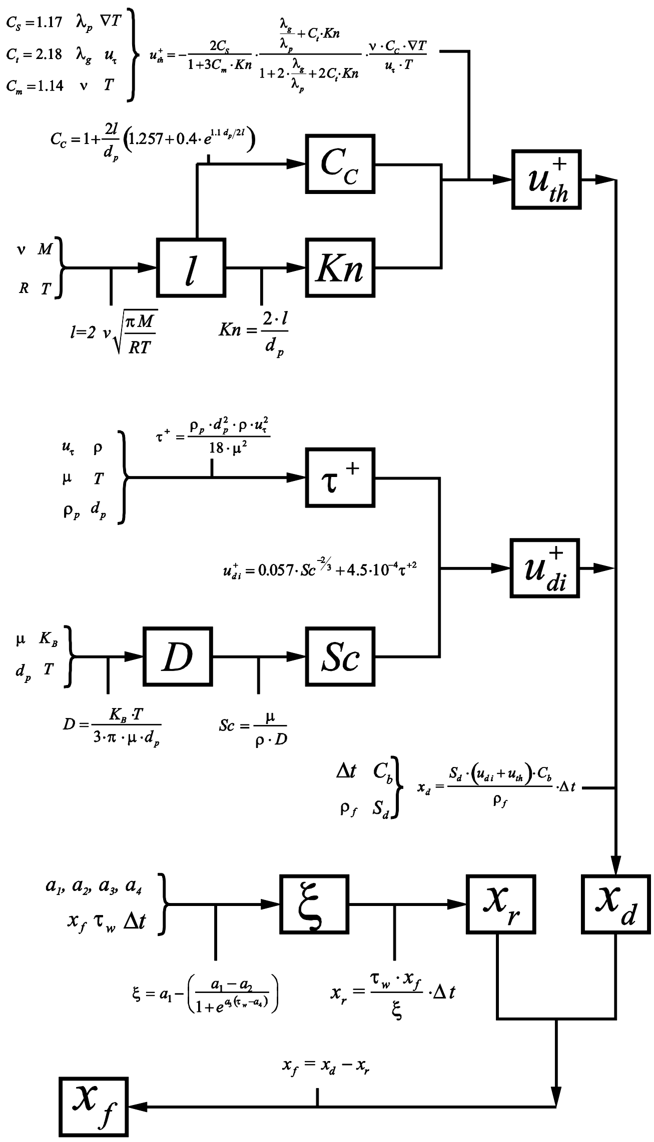

Fig. 2 Scheme of fouling model equations.

Based on the specific characteristics of the analysed flow (a low particle load, a low Stokes number, the present temporal scales, and the typical particulate size distribution in diesel exhaust systems) the following hypotheses have been proposed:

• The layer is homogenous with uniform properties. This assumption is commonly used in the literature. The fouling layer properties were estimated from experimental results: density ρ_f=36.5 kg/m^3 and conductivity λ_f=0.07 W/mK (Paz et al., 2009). Because these values were obtained experimentally, they can be considered to be the density and the thermal conductivity of an effective homogenous layer, although there is evidence indicating a stratified structure of this layer.
• An ideal gas with a constant particle concentration and a 100% sticking probability, S_d=1, was assumed. The bulk particulate concentration C_b was set to 10^{-3} kg/Nm^3 based on literature references (Grillot and Icart, 1997; Zhang et al., 2002).
• Particle impacts are negligible, and the fluid-solid interactions are unidirectional.
• The time evolution is a succession of quasi-steady stages.
• Sooting-type fouling occurs, so chemical reactions, condensation, solidification and corrosion have not been considered.
• Particles are removed by the shear stress mechanism and re-entrained in the gas flow.

NUMERICAL IMPLEMENTATION

The implementation and coupling of the proposed fouling model with a CFD program was performed using the commercial code ANSYS-FLUENT 6.3.26.

The fouling layer growth causes a reduction in the flow area, which causes an increase in pressure drop and the well-known efficiency reduction effect. This effect can change the mean flow conditions, even indirectly affecting the fouling process itself.

For example, El-Batsh (2001) studied three different numerical implementations of turbine blade fouling: the moving boundary concept, the filling and transformation of fluid cells, and reconstruction of the fouled profile. All approaches reproduce the profile change due to fouling but involve a complex mesh generation process and high computational cost.

The model presented in this paper provides an exhaust gas CFD fouling model implementation that accounts for the temporal and local evolution of the fouling thickness.

The physical concept of the deposition-removal process has been translated into increasing and decreasing processes of the computational fouling layer. The volume of each fluid cell adjacent to a wall is compared with the fouling thickness, which is calculated at every time step, and it is assumed that a cell is a fluid cell until the thickness reaches the top of the cell.

When the fouling thickness is larger than the fluid cell size, the fluid cell is converted externally into a solid with specific fouling properties. This simplification is possible provided that the height of each cell in the region near the wall is small enough. The height of the cells employed in this work was on the order of 10^{-3} times the tube diameter.

To perform this modification, a collection of user-defined functions, batch processes and subroutines were created to determine the volume of the cell, calculate the fouling thickness and run all of the operations required for making the decision about changing the type of the cell in real time. Once the cell adjacent to a wall is fouled, the growth process should continue in the cell above the fouled cell. Taking advantage of the prismatic mesh recommended for correct wall treatment of the flow, all of the information is transferred to the corresponding cell header, which drives the fouling growth of each column. The fouling layer grows until it fills up the cell; the numerical growth process is shown in the Fig. 3 (Suárez et al., 2010). For easier visualization, the heights of the cells are not to scale.

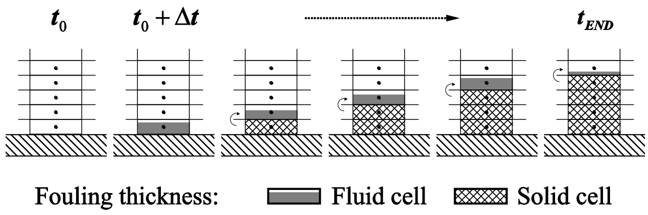

Fig. 3 Scheme of the numerical fouling growth methodology.

The fouling of each column was driven independently; however, to avoid a rough fouled surface, the deposition of each column was calculated as the average of its neighbours, which results in a smoother fouling profile. This averaging is required to maintain coherence between the spatial discretization and the local hydrodynamic conditions.

The thickness assigned to each cell is given by Eq. (13), which represents the weighted moving average.

$$x_{f,i} = \frac{x_{f,i-N} + ... + x_{f,i} + ... + x_{f,i+N}}{2N+1} \qquad (13)$$

This algorithm is repeated until the process reaches the asymptotic solution, which means that deposition and removal rates are balanced and that the effective deposition rate is zero.

To reproduce this evolution process until the asymptotic values are reached, the fouling process has been repeated at each time step until reaching the steady-state condition. Therefore, the numerical methodology is coupled to the flow solution by means of a sequential loop, which is summarized in Fig. 4. The time step was dynamically assigned to guarantee that at least one cell is clogged.

The process starts at the top of the scheme, assuming clean conditions, and it is solved with Fluent. Moving counter-clockwise around the graphic outline, the solid phase is calculated externally with the fouling model and the local CFD flow parameters. The mesh is then updated, and the loop is repeated until the asymptotic solution is reached. As a result, both the final thickness and the evolution of all of the parameters are calculated and recorded.

Recent computational efforts have focused on increasing the accuracy of turbulence modelling, which implies the use of finer grids in the wall regions because most advanced turbulent models impose very fine mesh sizes near the walls. Therefore, the number of cells in the boundary layer should almost always be high enough. To summarize, the numerical approach proposed in this research implies a further increase in the mesh size requirements, but the mesh size will be on the same order of magnitude as those used in enhanced-wall-treatment turbulence models.

This study specifically investigates fouling deposition in exhaust gas systems. To allow for experimental validation, the same cross-flow tubes used in the tested geometries have been simulated. The geometry and the mesh of the tested tubes were generated using GAMBITtm and T-GRID, which are the preprocessing modules of the Fluent code.

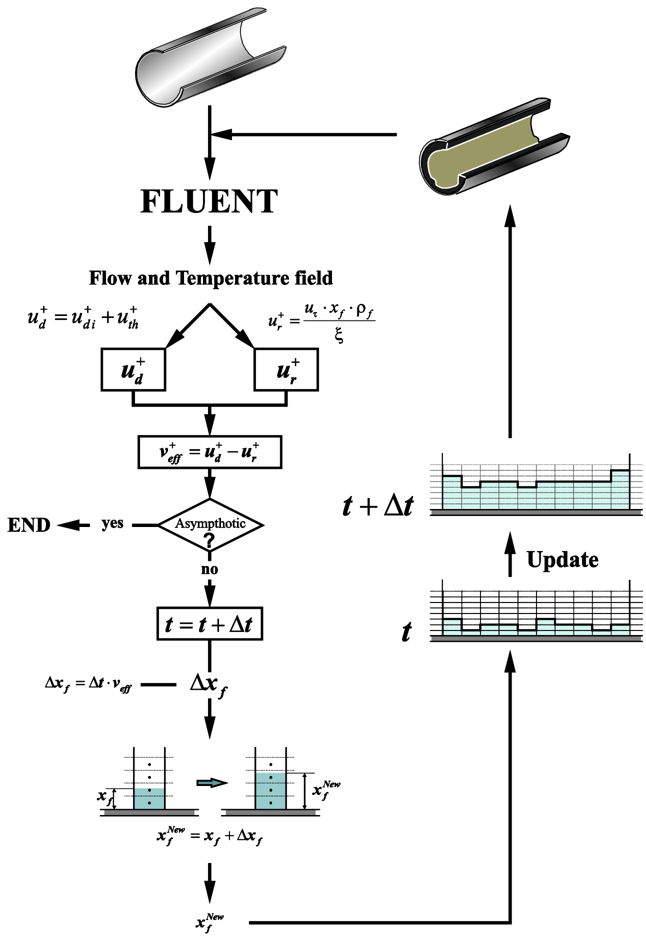

Fig. 4 Scheme of the sequential loop methodology.

To solve the fouling model in cells adjacent to the wall, two regions were constructed. The first region was the near-wall region with 50 levels and a uniform prismatic layer, with a size adjusted to attain a y^+ value for the cell adjacent to the wall of approximately 1. The second region contained 15 prismatic layers with linear growth, which produces a smoother transition. Once the resulting tube mesh model passes all quality checks, the mesh is exported to FLUENT, in which the boundary conditions and physical properties are set up. In this work, different grids were used to confirm the grid-independent solution, and stable results were obtained with a tube diameter–transverse cell size ratio on the order of 15, yielding a final mesh of ~10^6 cells. An Intel ® Xeon ® Quad-Core E5530 2.4 GHz cluster with 96 GB of RAM was used for the computation. More details about the computational implementation can be found in E. Suárez (2010).

RESULTS AND DISCUSSION

The tubes were tested under different operating conditions, with different gas mass flows rates and coolant temperatures. More details about the experimental configuration can be found in M. C. Paz et al. (2009).

The experimental fouling thickness results were obtained after reaching the asymptotic condition. The proposed model has been applied to a tube inserted transversely to the flow tube under the same conditions.

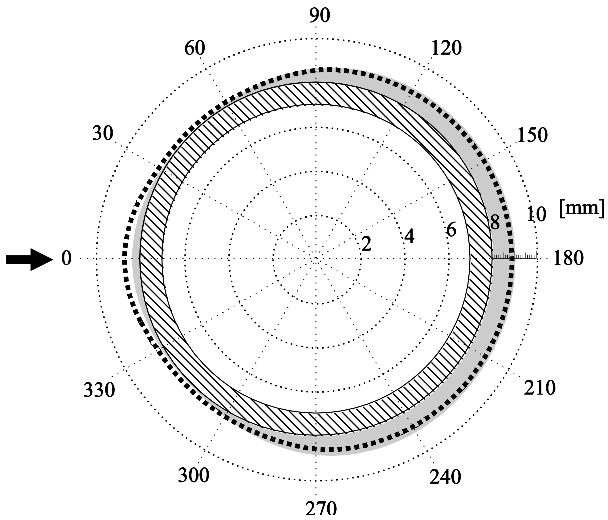

Fig. 5 Experimental fouling deposit (grey contour) and model prediction (dotted line).

The experimentally measured fouling thicknesses on the outside of the middle transverse tube section are compared with the asymptotic profiles predicted by the CFD fouling model. An example result is shown in Fig. 5. In this figure, the fouling profiles in polar coordinates are compared. The error was calculated as the difference between the model and experimental thickness at each angular position.

The total average error in the fouling thickness is less than 6%. The CFD model shows good agreement with the experimental data in terms of its ability to predict overall and local fouling behaviour and rates. Fig. 6 shows a comparison between the predicted fouling profiles and the experimental results.

The weighed and predicted fouling masses were also compared. The corresponding values are detailed in table 1.

Table 1. Experimental and model results for the mass deposited on the gas side of the tested tubes.

Test number	Experimental	Model
I	45.7	46.2
II	27.4	28.0
III	27.5	26.0
IV	17.3	17.8
V	33.0	36.0

VI	26.9	24.8
VII	11.1	10.8
VIII	15.1	16.7

In Fig. 7, a comparison of the temporal evolution of the deposited fouling layer predicted by the model is shown at *0%*, *10%*, *25%*, *50%* and *100%* of the asymptotic time, from bottom to top, respectively. The fouling is depicted by a black contour. The isolines of the flow show the flow pattern as the soot layer thickness increases.

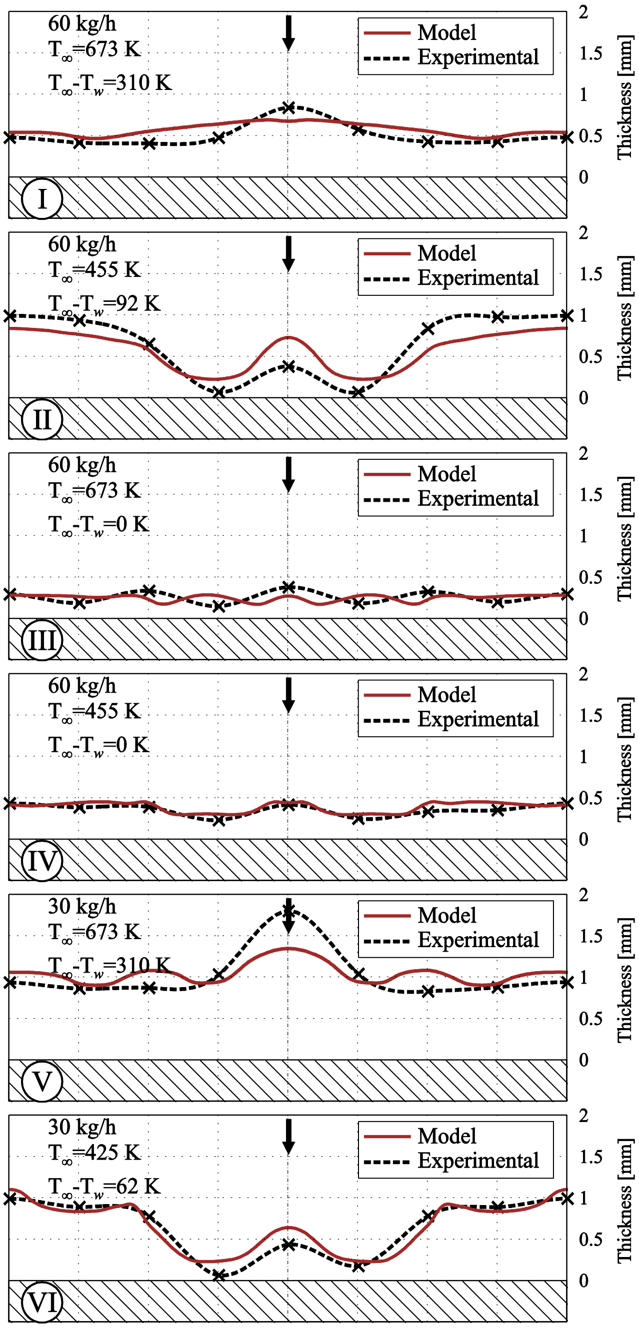

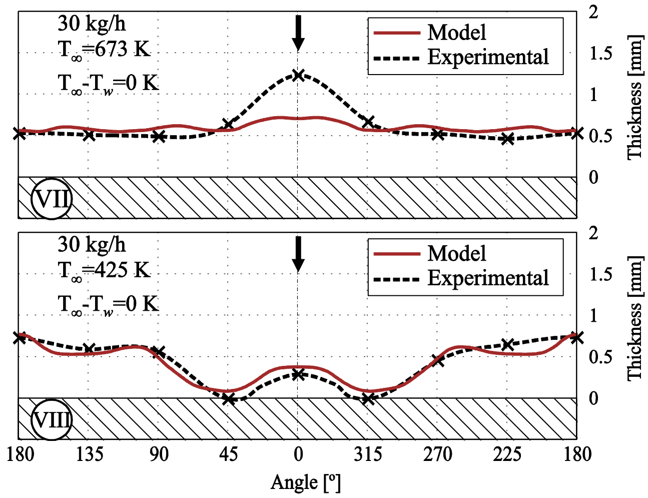

Fig. 6 Experimental versus CFD-predicted fouling profiles.

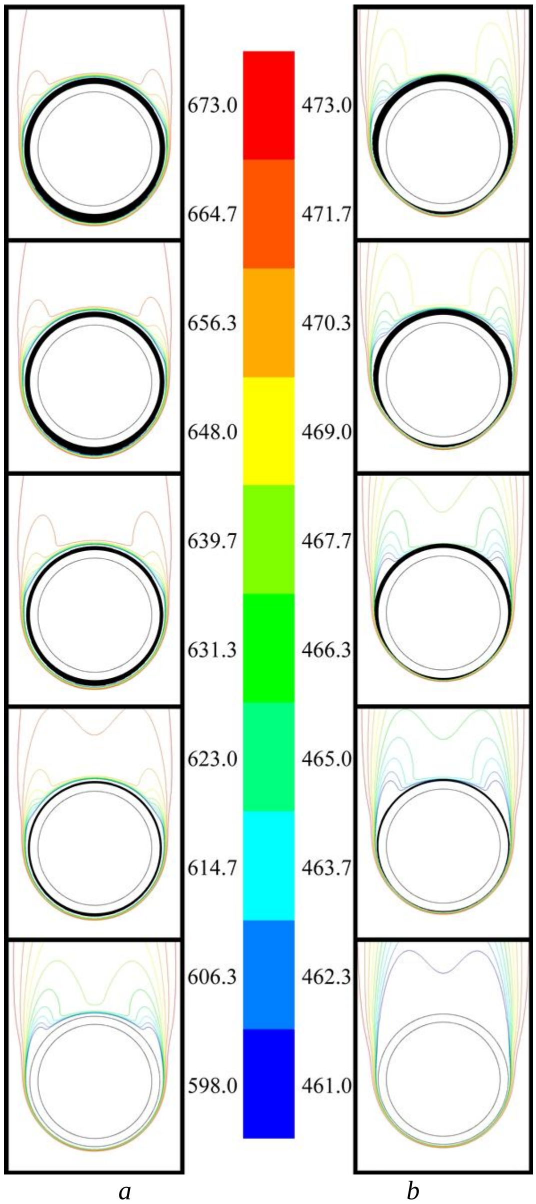

Fig. 7 Temporal fouling evolution coloured by temperature contour [K], *a)* $Re=2.2\cdot10^3$ and $\nabla T_{max}=1.85\cdot10^6$ K/m, *b)* $Re=2.8\cdot10^3$ and $\nabla T_{max}=6.23\cdot10^6$ K/m.

An important dependence between the final deposited thickness and the temperature gradient has been found. To explain this effect, the dimensionless deposition velocities with and without a temperature gradient at the beginning of the process are depicted in Fig. 8. A significant increase can be seen due to the thermophoresis contribution.

The increase in the deposition velocity associated with thermophoresis is fundamental (Paz et al., 2009) and is particularly intense for the submicron soot particles typically found in diesel exhaust gases (Eastwood, 2008; Kittelson, 1998). Moreover, the maxima are in the largest shear stress areas, near *60º* and *-60º*, where the higher dimensionless particulate relaxation times are found.

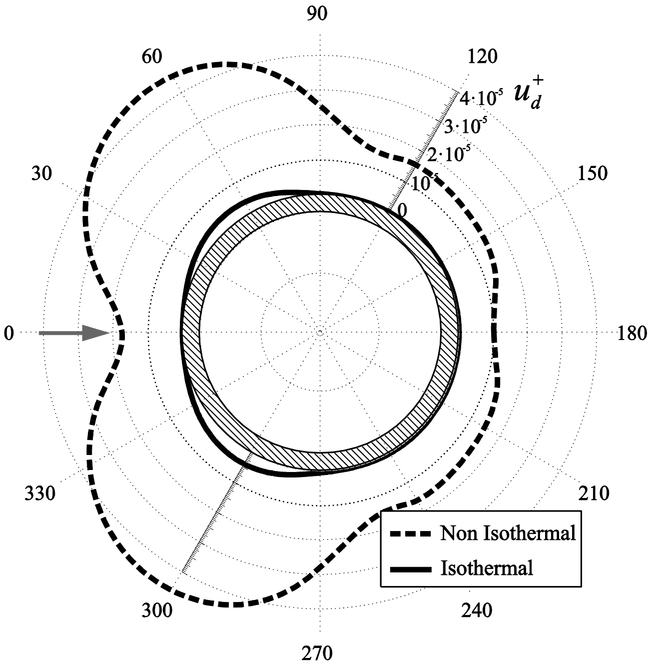

Fig. 8 Dimensionless deposition velocities.

CONCLUSIONS

The following conclusions can be made with respect to the methodology proposed in this work:

1. Each fully fouled cell is converted into a solid. As a result, the real fouling geometry is obtained and modelled; therefore, this approach makes it possible to account for the reduction in the cross-sectional area.
2. The computational model cost is considered to be affordable, an important initial requirement, and the numerical model developed could be very useful to compare different, previously proposed fouling models because the algorithm is independent of the set of model equations.
3. The effect of thermophoresis in the tests used for validation emphasizes the importance of the temperature gradient on particulate deposition in exhaust gas systems.
4. The detail provided by the CFD fouling model demonstrates that the growth of the soot layer has a considerable impact on the hydrodynamics of the system, and vice versa.
5. As a final conclusion, this Euler-0D model and its numerical implementation represent a valuable tool for the prediction of the main aspects of the performance of exhaust gas devices exposed to fouling.

NOMENCLATURE

a_i Experimentally fit constants, dimensionless
A Asymptotic fouling model constant, m^{-2} K^{-1} W s
B Asymptotic fouling model constant, s^{-1}
C_b Bulk particle concentration, kg m^{-3}
C_C Stokes-Cunningham slip correction factor, dimensionless
$C_{t,m,s}$ Thermophoresis constants, dimensionless
d_p Particulate diameter, m
D Mass diffusivity, m^2 s^{-1}
FF Fouling factor, m^2 K W^{-1}
Kn Knudsen number, dimensionless
l Mean free path, m
Sc Schmidt number, dimensionless
S_d Sticking probability, dimensionless
t Time, s
T Temperature, K
u^+_{di} Isothermal deposition velocity, dimensionless
u^+_{th} Thermophoretic deposition velocity, dimensionless
u_τ Fluid friction velocity, m s^{-1}
v^+_{eff} Effective deposition velocity, dimensionless
U Global heat transfer coefficient, m^{-2} K^{-1} W
x_f Fouling thickness, m
λ Conductivity, W m^{-1} K^{-1}
ρ Density, kg m^{-3}
τ_w Wall shear stress, Pa
τ^+ Dimensionless relaxation time
υ Kinematic viscosity, m^2 s^{-1}
ξ Strength bond factor, kg m^{-1} s^{-1}

Subscript

c clean
d deposition
f fouled
g gas
r removal
w wall
∞ mean flow

Superscript

\+ Dimensionless
* Asymptotic

REFERENCES

M. Abarham, J. Hoard, D. Assanis, D Styles, E. W. Curtis and N. Ramesh. Review of soot deposition and removal mechanisms in EGR coolers. Society of Automotive Engineers, 2010-01-1211.

M. S. Abd-Elhady, S. Abd-Elhady, C. C. M. Rindt, and A. A. v. Steenhoven, 2009, Removal of gas-side particulate fouling layers by foreign particles as a function of flow direction. Applied Thermal Engineering, Vol. 29, pp. 2335 - 2343.

I. Adhiwidjaja, S. Matsusaka, H. Tanaka, and H. Masuda, 2000, Simultaneous phenomenon of particle deposition and reentrainment: Effects of surface roughness on deposition layer of striped pattern. Journal of Aerosol Science, Vol. 33, pp. 323-333.

T. R. Bott, 1995, Fouling of Heat Exchangers. Elsevier Ltd, pp. 522.

D. Bouris, E. Konstantinidis, S. Balabani, D. Castiglia, and G. Bergeles, 2005, Design of a novel, intensified heat exchanger for reduced fouling rates. International Journal of Heat and Mass Transfer, Vol. 48, pp. 3817 - 3832.

M. F. Chandler, Y. Teng, and U. O. Koylu, 2007, Diesel engine particulate emissions: A comparison of mobility and microscopy size measurements. Proceedings of the Combustion Institute, Vol. 31, pp. 2971 - 2979.

P. Eastwood (2008). "Particulate Emissions from Vehicles." John Wiley and Sons, Ltd.

H. El-Batsh (2001). Modelling particle deposition on compressor and turbine blade surfaces. PhD Thesis. Vienna University of Technology.

N. Epstein, 1997, Elements of particle deposition onto nonporous solid surfaces parallel to suspension flows. Experimental Thermal and Fluid Science, Vol. 14, pp. 323 - 334.

S. K. Friedlander, 1977, Smoke, dust and haze, fundamentals of aerosol behavior. John Wiley & Sons, Inc., pp. 317-333.

S. K. Friedlander, and H. F. Johnstone, 1957, Deposition of Suspended Particles from Turbulent Gas Streams. Industrial and Engineering Chemistry, Vol. 49 (7), pp. 1151-1156.

J. M. Grillot, and G. Icart, 1997, Fouling of a cylindrical probe and a finned tube bundle in a diesel exhaust environment. Experimental Thermal and Fluid Science, Vol. 14, pp. 442 - 454.

A. Guha, 1997, A unified Eulerian theory of turbulent deposition to smooth and rough surfaces. Journal of Aerosol Science, Vol. 28, pp. 1517 - 1537.

J. Hoard, M. Abarham, D. Styles, J. M. Giuliano, C. S. Sluder, and J. M. E. Storey, 2008, Diesel EGR Cooler Fouling. Society of Automotive Engineers, Vol. 01-2475.

D. Q. Kern, and R. E. Seaton, 1959, A theoretical analysis of thermal surface fouling. British Chemical Engineering, Vol. 4, pp. 258-262.

N.-H. Kim, and R. L. Webb, 1991, Particulate fouling of water in tubes having a two-dimensional roughness geometry. International Journal of Heat and Mass Transfer, Vol. 34, pp. 2727 - 2738.

D. B. Kittelson, 1998, Engines and nanoparticles: a review. Journal of Aerosol Science, Vol. 29, pp. 575 - 588.

W. J. Marner, 1990, Progress in Gas-Side Fouling of Heat-Transfer Surfaces. Applied Mechanics Reviews, Vol. 43, pp. 35-66.

S. Matsusaka, M. Koumura, and H. Masuda, 1997, Analysis of adhesive force between particle and wall based on particle reentrainment by airflow and centrifugal separation. Kagaku Kogaku Ronbunshu, Vol. 23, pp. 561-568.

H. M. Müller-Steinhagen, and J. Middis, 1989, Particle Fouling in Plate Heat Exchanger. Heat Transfer Engineering, Vol. 10 nº4, pp. 30-36.

M. C. Paz, E. Suárez, A. Eirís, and C. Castaño (2009). 10th Conference on Energy for a Clean Environment, Lisbon.

E. Suárez, C. Paz, J. Porteiro, and A. Eirís (2010). Simulation of the fouling layer evolution in heat transfer surfaces. In "V European Conference on Computational Fluid Dynamics", Lisbon.

E. Suárez (2010). Modelado y simulación de la deposición de partículas en flujos bifásicos turbulentos disperos en presencia de gradientes de temperatura. Aplicación a enfriadores de gases de escape, (In Spanish). PhD Thesis, University of Vigo, Spain.

L. Talbot, R. K. Cheng, R. W. Schefer, and D. R. Willis, 1980, Thermophoresis of particles in a heated boundary layer. Journal of Fluid Mechanics, Vol. 101 part 4, pp. 737-758.

W. Theerachaisupakij, S. Matsusaka, Y. Akashi, and H. Masuda, 2003, Reentrainment of deposited particles by drag and aerosol collision. Journal of Aerosol Science, Vol. 34, pp. 261 - 274.

B. Thonon, S. Grandgeorg, and C. Jallut, 1999, Effect of Geometry and Flow Conditions on Particulate Fouling in Plate Heat Exchangers. Heat Transfer Engineering, Vol. 20, N 3.

C.-J. Tsai, and H.-C. Lu, 1995, Design and Evaluation of a Plate-to-Plate Thermophoretic Precipitator. Aerosol Science and Technology, Vol. 22:2, pp. 172-180.

N. B. Wood, 1981, A simple method for the calculation of turbulent deposition to smooth and rough surfaces. Journal of Aerosol Science, Vol. 12, pp. 275 - 290.

J. Young, and A. Leeming, 1997, A theory of particle deposition in turbulent. Journal of Fluid Mechanics, Vol. 1 340, pp. 129-159.

Z. Zhang, S. L. Yang, and J. H. Johnson, 2002, Modeling and numerical simulation of diesel particulate trap performance during loading and regeneration. Society of Automotive Engineering, Vol. 2002-01-1019.